Meng, F., Mavromatis, A., Bi, Y., Wang, R., Yan, S., Nejabati, R., & Simeonidou, D. (2019). Self-Learning Monitoring On-Demand Strategy for Optical Networks. *IEEE/OSA Journal of Optical Communications and Networking*, *11*(2), A144-A154. Article 8657333. https://doi.org/10.1364/JOCN.11.00A144

A Self-Learning Monitoring On-Demand Strategy for Optical Networks [Invited]

Fanchao Meng, Alex Mavromatis, Yu Bi, Rui Wang, Shuangyi Yan, Reza Nejabati and Dimitra Simeonidou

***Abstract*—In current dynamic optical networks with cascaded filters and amplifiers, optical signal-to-noise ratio (OSNR) can vary significantly from channel to channel. Under such uncertainty, OSNR prediction for unestablished channels becomes indispensable but remains a big challenge. For protective network planning purposes such as margin threshold setting or wavelength assignment, it is desirable to evaluate the worst OSNR performance of each network link. Such exploration will unavoidably employ active monitoring probes which may cause interruptions to the network. An efficient active monitoring strategy that optimizes the choice of probes or monitoring trials is needed. We propose a "self-learning" monitoring strategy integrated at intermediate nodes. Our method can intelligently select the channel to be monitored in order to search for the target global maxima of OSNR degradation for a specific link. Our monitoring scheme detects intermediate node OSNR in the linear regime. It is shown that our method can predict the target OSNR value with only 0.5dB error while reducing the required monitoring data by up to 91% compared with conventional methods.**

***Index Terms*—Artificial intelligence, optical performance monitoring, OSNR, optical networking, Bayesian optimization.**

I. Introduction

THE emergence of heterogeneous quality of service (QoS) requirements from applications continues to drive the evolution of traditional optical networks. Advanced technologies such as flexible transponders [1], coherent transmission [2] and re-configurable optical add-drop multiplexers (ROADMs) [3] have considerably enhanced the network dynamicity and flexibility. Offline network planning methods are mainly developed under static optical transmission models, so they have difficulty in capturing such complex system behavior [4]. The advances of various optical performance monitoring (OPM) technologies have made the optical network fully cognitive, i.e., being able to perceive real-time optical performance and feed the information back to the control plane. The most critical feature that represents the quality of transmission (QoT) is the optical signal-to-noise ratio (OSNR) [5]. Therefore, OSNR monitoring is imperative and should be placed ubiquitously across the physical layer.

In current coherent receivers, OSNR can easily be computed by the statistical-moment based or the error-vector-magnitude (EVM) based methods that can measure lightpath-level performance [5]. However, reliable and distributed in-band OSNR monitoring is also needed at intermediate nodes (e.g., ROADMs). for obtaining link-level information. Due to the lack of intermediate node monitoring, previous research proposes to combine active monitoring with "network kriging" [6] in order to measure unestablished lightpath performance. It works by indicating the minimum number of informative monitoring probes in order to maximize the network knowledge gain. Although this approach proves to be effective, the assumption that impairments are flat across the transmission spectrum may influence the prediction accuracy [7]. Such uncertainty problem will be addressed in this paper. Moreover, the computational complexity of network kriging is high for large networks [8]. Therefore, we propose an alternative method, i.e., intermediate node monitoring, to solve the network uncertainty at link level. It is capable of providing straight-forward intermediate node OSNR information that can potentially enable low-complexity link-level network planning. Relevant work has been demonstrated in a field trial in reference [9].

For the purpose of designing a network with efficient self-diagnose capability, it is not necessary to monitor the entire network. As the network expands, large amounts of data will be generated from the ubiquitous monitoring devices across the network. This may cause additional operational load of the network control plane due to finite flow entries [10], [11]. The aforementioned data is not only restricted to QoT estimation, but also to offline machine/deep learning training and cross-layer network optimization. The latter may require data from the past or from different network layers. On the other hand, probe signals are often utilized for active monitoring purposes [6], [12] which can cause additional interference and blocking with existing network services [13], [14]. Since sending probe signal is both operationally expensive and impactive to network performance, it is desirable to minimize the number of probes or monitoring trials. The strategy used in this paper assumes that no probe is required if there is an established connection, otherwise probe channels may be used for unestablished connections.

Besides optimizing active monitoring trials, network diagnosis also needs to be agile and real-time. In the case of end-to-end coherent service provisioning, the OSNR of each channel can be monitored simultaneously by each corresponding receiver as a DSP by-product [5]. However, for intermediate nodes where a single OSNR monitoring device is deployed, the OSNR of each channel cannot be monitored simultaneously. As such, sharing the intermediate-node monitoring device among multiple channels remains an unsolved challenge. For proactive network planning, the worst OSNR performance of the link is critical to be tracked. Failures can be proactively

M. Shell was with the Department of Electrical and Computer Engineering, Georgia Institute of Technology, Atlanta, GA, 30332 USA e-mail: (see http://www.michaelshell.org/contact.html).

J. Doe and J. Doe are with Anonymous University.

Manuscript received April 19, 2005; revised August 26, 2015.

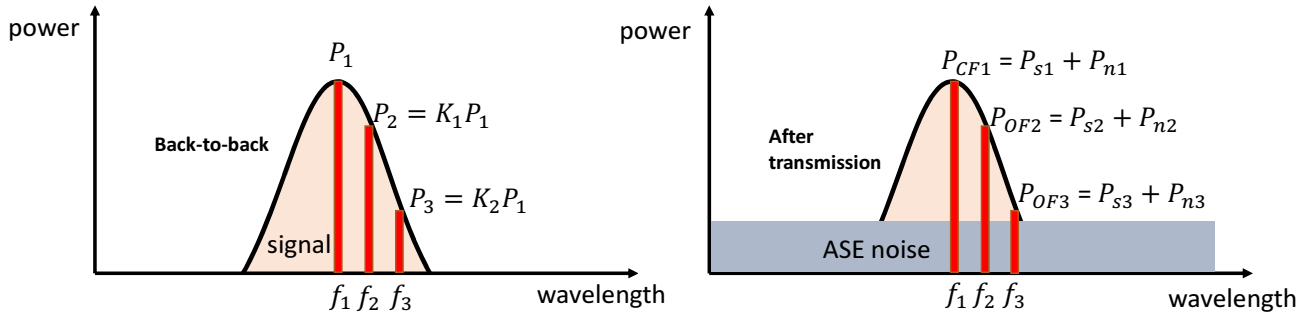

(a) Offset-frequency in-band OSNR monitoring

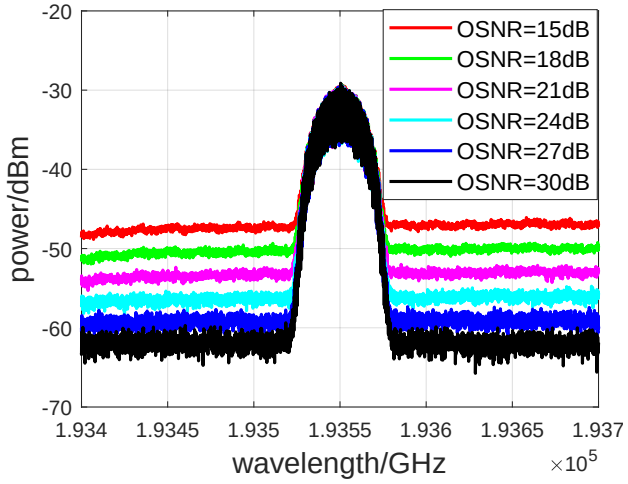

(b) ASE noise loading

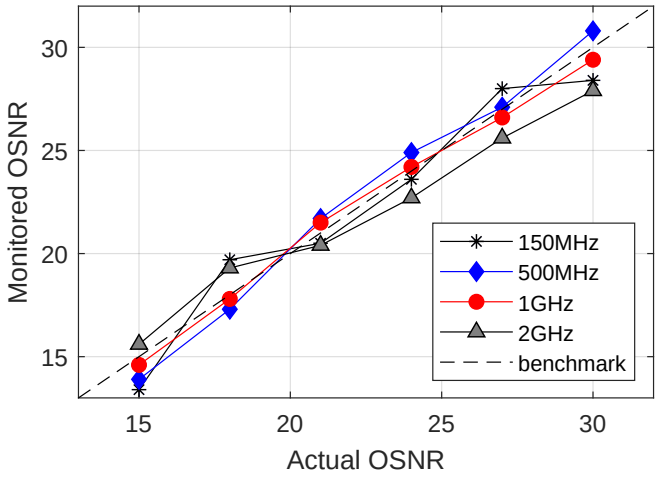

(c) In-band OSNR monitoring accuracy

Figure 1: (a) Offset frequency power monitoring method to compute in-band OSNR, the back-to-back spectrum is used to determine parameters K_1, K_2, ASE noise is assumed to be flat within the channel bandwidth. (b) Coupling additional ASE noise into signal to emulate OSNR degradation and calibrate parameters for α, β, c. (c) In-band OSNR monitoring accuracy, 1GHz resolution gives the best accuracy with $\pm 0.6dB$ error.

avoided once the worst OSNR degradation case is addressed. It can be used as a satisficing constraint (no more than the worst case threshold) when performing wavelength assignment and routing. The state-of-the-art erbium-doped fiber amplifier (EDFA) comes with intrinsic gain and noise figure (NF) spectrum non-uniformity characteristics. This further contributes to OSNR non-uniformity across the C-band [15], [16]. Even under static gain equalization control, EDFA power excursion and offset filtering problems also lead to OSNR uncertainty [17]. Such uncertainty is difficult to formulaically analyze. Furthermore, the network status can change quickly due to dynamic add-drops, which makes the system a "black box". Instead of conducting complete examination of the black box, intelligent monitoring strategies are required to search for the worst OSNR performance of a link with as few monitoring trials as possible.

Unlike previous work which applies offline machine learning techniques (using hand-crafted training set) for predictions [18], our proposed learning method utilizes online monitoring data to update the training process in real-time. Such online, sustained learning is intrinsically adaptable to dynamic, variational systems like ours. Similar online learning is also proposed in [19]. However, the authors average the path-level OSNR difference between the prediction and monitoring data to each cascading span. Such per-span OSNR update rule of [19] is likely to spread one particular span degradation to multiple spans which can lead to under-estimation of per-span (or per-link) OSNR performance.

In previous work [20], we presented and demonstrated the monitoring-on-demand (MoD) strategy at intermediate nodes to eliminate redundant OPM data from the physical device where a 100G-based 50 GHz-spaced 16-channel system was operated in a cross-city field trial. The number of monitoring trials needed to find the global maximum OSNR degradation of a link is significantly reduced by applying Bayesian optimization (BO). We expand the work by further demonstrating that pure Gaussian process (GP) learning without BO requires much more monitoring data for our prediction purpose. We also report and test the algorithm integrated in the MoD intermediate node for computing the in-band OSNR of DP-QPSK signals. This paper is organized as follows: Section II describes the in-band OSNR monitoring function implemented at intermediate nodes. Section III gives detailed explanation of the monitoring strategy enabled by the GP and BO algorithms.

In Section IV we demonstrate the advantage of the proposed solution in a field trial experimental setup. And finally Section V summarizes the work.

II. Integrating in-band OSNR monitoring at intermediate nodes

In-band OSNR monitoring in principle should be modulation format (MF) independent and tolerant to spectrum narrowing effect. The latter is induced by cascaded wavelength selective switches (WSS). We apply a reference optical spectrum based OSNR monitoring algorithm [21]–[23] using a high-resolution optical spectrum analyzer (OSA). This method has been proven to be MF independent and WSS filtering effect insensitive. In real applications this monitoring function can be implemented using lower cost coherent reception and an RF measurement device [22], [23]. To realize physical layer autonomous in-band OSNR monitoring, single channel filtering is important so that the algorithm can autonomously locate the central frequency by searching for the maximum power (as there is only one channel). Then accurate offset frequencies can be accordingly located. It is worth noting that there actually exist many methods in the literature to monitor the in-band OSNR. For example, the delay-line interferometer (DLI) based methods [24], [25] which are based on single channel monitoring. We address the feasibility of integrating this monitoring function into ROADMs leveraging the architecture-on-demand (AoD) concept [26]. Our proposed MoD algorithm is not restricted to monitoring with an OSA, it aims to be applicable to other in-band OSNR monitoring techniques as well.

A. In-band OSNR monitoring algorithm

Fig. 1(a) shows the working principle of the algorithm. The signal spectrum before transmission is monitored back-to-back as the reference. Three signal spectral powers P_1, P_2 and P_3 are measured at three frequencies f_1, f_2, f_3 within the signal band. f_1 is the center frequency and f_2, f_3 are two offset frequencies. The power ratios $K_1 = P_2/P_1$ and $K_2 = P_3/P_1$ are determined from the reference spectrum. After transmission, the signal OSNR will be degraded mainly by amplified spontaneous emission (ASE) noise which can be modeled as white Gaussian noise. Two parameters α and β are introduced to model WSS filtering penalty on the signal spectrum. By monitoring the spectral powers $P_{CF1}, P_{OF2}, P_{OF3}$ after transmission, we have [22]

$$P_{CF1} = P_{s1} + P_{n1} \tag{1}$$

$$P_{OF2} = P_{s2} + P_{n2} = K_1\alpha^N P_{s2} + P_{n1} \tag{2}$$

$$P_{OF3} = P_{s3} + P_{n3} = K_2\beta^N P_{s3} + P_{n1} \tag{3}$$

N is the number of filters the signal traversed, P_{s1}, P_{s2}, P_{s3} are signal power at f_1, f_2, f_3 respectively, and P_{n1} is the ASE noise power at f_1, f_2, f_3. Solving the above equations gives the value of P_{s1} and P_{n1} hence OSNR can be computed as

$$OSNR_{dB} = 10log[c\frac{P_{s1}}{P_{n1}}] \tag{4}$$

where $c = 1.7$ is a calibration coefficient which depends on device power monitoring sensitivity and WSS filter setting [22], [23].

B. Monitoring performance

By conducting back-to-back ASE noise loading for 32GBaud dual-polarization QPSK signals, the performance of the in-band OSNR algorithm using Finisar WaveAnalyzer 1500S [27] is evaluated. 50GHz fixed grid is used for each channel spacing. Different OSNR levels after transmission are emulated by coupling additional ASE noise into the signal as shown in Fig. 1(b). The OSNR value ranges from 15dB to 30dB. As there is no intermediate filtering, N is set to 0, hence $\alpha^N = \beta^N = 1$. The choices of two spectral power measurement frequencies f_2, f_3 are set at $f_2 = f_1 + 20GHz$, $f_3 = f_1 + 23.5GHz$ according to [22]. The WaveAnalyzer (WA) frequency resolution is set to 150MHz, 500MHz, 1GHz, 2GHz to explore the accuracy of the monitoring performance. Out-of-band OSNR computation is used to obtain the benchmark which is used to assess the monitoring performance [28]. As shown in Fig. 1(c), 1GHz resolution gives the best OSNR monitoring accuracy with maximum error of 0.6dB while other resolution settings have worse accuracy. Theoretically, finer resolution should give better accuracy [22], but due to the WA device sensitivity at finer frequency resolution ($\pm 1GHz$ error), the spectral power reading at the nominal frequency is not stable with 150MHz or 500MHz. So 1GHz resolution is used to relax the sensitivity issue. Such power-based OSNR monitoring technique only considers ASE noise induced by EDFAs, nonlinear noise is not considered.

C. Node architecture supporting the monitoring on-demand

Fig. 2 shows the hardware implementation supporting monitoring on-demand (MoD) function in the optical backplane switch. The optical switch is an essential element in ROADMs [29]. It is worth noting that the monitoring function can also be installed at any point of the network, for example, an inline EDFA output port. But this will result in the device being only able to monitor a single route. The key components are tap coupler, WSS (or programmable optical filter) and WA. All the devices are pre-connected in the programmable optical switch. The signal power is tapped from the traffic port and then fed into the WSS. The filter (bandpass with central frequency and bandwidth) is re-configured dynamically to choose the channel of interest for monitoring. WA is connected to the output of the WSS for in-band OSNR computation. The central and offset frequencies are autonomously located by searching for the spectrum peak power. Monitoring parameters $K_1, K_2, \alpha, \beta, c$ are pre-calibrated and stored locally in the device controller. The controller computes the OSNR value of the current channel and dynamically re-configures the filter to choose the next channel of interest. The process of making the re-configuration decision follows the Bayesian optimization learning model. The decision is influenced by the OSNR performance it has monitored so far.

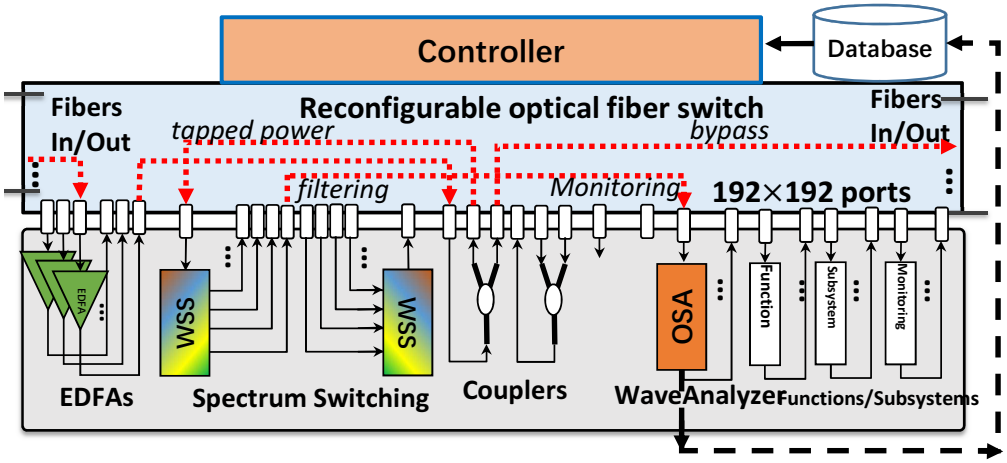

Figure 2: Monitoring on-demand physical architecture where all programmable devices are pre-connected in the optical switch integrated in ROADMs for dynamic on-demand switching. Signal power is tapped and then filtered by a WSS to choose the channel of interest for OSNR monitoring.

III. Monitoring strategy enabled by learning

Empirically the OSNR of a target channel can be estimated by monitoring other channels with the same route but at different wavelengths. However, the ASE noise spectrum non-uniformity has to be properly addressed. In optical transmission links, each individual EDFA comes with inherent gain and NF spectrum non-uniformity [30]. Even under static power equalization [31], [32], each EDFA is likely to have undetected gain/NF perturbations and power excursions due to ageing, pump power condition, dynamic loading, temperature, etc [17], [33]–[35]. This non-uniformity problem gets even worse after cascading many independent EDFAs in a transmission link. This causes distant wavelengths to be less OSNR-representative than the neighboring ones. As it is analytically intractable to parameterize the ASE spectrum in dynamic optical networks, machine learning (ML) models can be used to "learn" from monitoring data.

A. Gaussian process inference

As uncertainties happen during network operation, offline training ML models are not suitable to capture the online system characteristics [17], [36]. As such, GP is considered for online learning with a limited data set [37]. Online learning means the system can take real-time data as the training set to achieve sustained learning throughout the network lifecycle. Unlike weight-space ML methods such as linear regression which can easily underfit or overfit the training data, GP is a function-space kernel-based regression method. GP samples stochastic probability distributions in the function space. Such a flexible non-parametric model can represent the stochastic OSNR uncertainty obliquely but rigorously through monitoring.

To fit the GP model, the monitoring data (OSNR vs λ) of the existing channels is taken as the training set where λ is the channel wavelength. It is assumed that services are established one by one. So each time a new lightpath is established, its monitoring data is taken into the training set for prediction of the next single channel establishment., i.e., online training. The monitoring data is intrinsically noisy because the OSNR readings fluctuate around the mean value over time, as shown in Fig. 3. GP models additive independent and identically distributed (IID) Gaussian noise ϵ to the mean value such that [38]

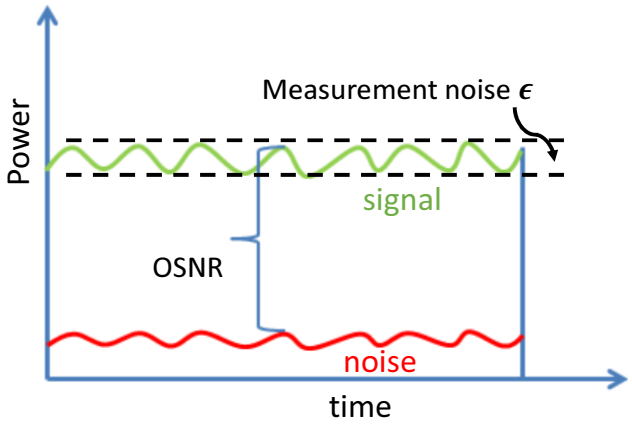

Figure 3: Additional measurement Gaussian noise ϵ is added to the training set.

$$Q(monitored) = Q(mean) + \epsilon \tag{5}$$

$$\epsilon \sim \mathcal{N}(0, \sigma_Q^2) \tag{6}$$

where Q(mean) is the mean OSNR value and σ_Q^2 is the measurement noise variance. Hence all future inferences are made by taking the measurement noise variance into account. The final fitted GP curve does not necessarily pass through each training point, but is always within the variance range σ_Q^2.

We model the similarity kernel (covariance function) using the squared exponential kernel or so called radio basis function (RBF) [39]

$$k(\lambda,\lambda^{'}) = \sigma_f^2 exp\left(\frac{-(\lambda-\lambda^{'})^2}{2l^2}\right) + \sigma_Q^2\delta(\lambda,\lambda^{'}) \tag{7}$$

where σ_f^2 (signal variance) and l (length scale) are hyperparameters that affect the shape and smoothness of GP. $\delta(\lambda,\lambda^{'})$ is the Kronecker delta function. The kernel function value $k(.,.)$ is a scalar which measures the similarity between two points. We use cosine similarity to measure correlation. If two channels are too far away, then $\lambda-\lambda^{'}$ goes to infinity, thus the kernel becomes 0 ($exp(-infinity) = 0$). This means that these two channels have little correlation (k is close to 0). In other words, closer channels offer more information to the OSNR estimation of target channel than distant channels. If there are m channels used as the training points, a m-by-m covariance kernel matrix $\mathbf{K}$ (throughout the paper matrices are shown in **bold** font) can be constructed as

$$\mathbf{K} = \begin{bmatrix} k(\lambda_1,\lambda_1) & k(\lambda_1,\lambda_2) & \cdots & k(\lambda_1,\lambda_m) \\ k(\lambda_2,\lambda_1) & k(\lambda_2,\lambda_2) & \cdots & k(\lambda_2,\lambda_m) \\ \vdots & \vdots & \ddots & \vdots \\ k(\lambda_m,\lambda_1) & k(\lambda_m,\lambda_2) & \cdots & k(\lambda_m,\lambda_m) \end{bmatrix} \tag{8}$$

The diagonal elements of $\mathbf{K}$ measure the self-similarity of each channel and are hence equal to 1. The amount of correlation between the training and test channels follows a joint multivariant Gaussian distribution (throughout the paper, "training channels" and "training points" are used interchangeably). The correlation is computed from the training set $\mathbf{Q}$ and test data Q_* according to the prior (initial belief of the sampled hidden function) [38]

$$\mathbf{K}* = \begin{bmatrix} k(\lambda_*,\lambda_1) & k(\lambda_*,\lambda_2) & \cdots & k(\lambda_*,\lambda_m) \end{bmatrix} \tag{9}$$

$$\mathbf{K}_{**} = k(\lambda_*,\lambda_*) \tag{10}$$

$$\begin{pmatrix} \mathbf{Q} \\ Q_* \end{pmatrix} \sim \mathcal{N}\left(\mathbf{0}\ , \begin{bmatrix} \mathbf{K} & \mathbf{K}_*^{\mathbf{T}} \\ \mathbf{K}_* & \mathbf{K}_{**} \end{bmatrix} \right) \tag{11}$$

where $\mathbf{K}_*$ is a 1-by-m matrix, $\mathbf{Q}$ is a m-by-1 matrix, $\mathbf{K}_*^{\mathbf{T}}$ is the transpose of $\mathbf{K}_*$. The posterior OSNR estimation of the test set Q_* conditioned on the training set $\mathbf{Q}$ and test input λ_* follows the following Gaussian distribution [38]

$$Q_*|(\mathbf{Q},\lambda,\lambda_*) \sim \mathcal{N}(\mu_*,\sigma_*) \tag{12}$$

$$\mu_* = \mathbf{K}_*\mathbf{K}^{-1}\mathbf{Q} \tag{13}$$

$$\sigma_* = \mathbf{K}_{**} - \mathbf{K}_*\mathbf{K}^{-1}\mathbf{K}_*^{\mathbf{T}} \tag{14}$$

The pseudocode that summarizes the GP algorithm fitting the transmission system is shown in Algorithm 1. The hyperparameters are optimized by maximizing the log marginal likelihood (maximum likelihood). It is maximized by seeking partial derivatives with respect to σ_f^2 and l.

An important feature of GP is that it computes an estimation confidence integral (ECI) that forms critical constraints for control decision making [37]. ECI quantifies posterior prediction uncertainty which goes high where there is no monitoring data, and goes low where there is sufficient monitoring data. 95% pointwise ECI is a common choice [38]

Input:
λ - - training channel wavelength (established connections);
$\mathbf{Q}$ - - training set OSNR (established connections);
$\mathbf{K}$ - - kernel function;
σ_Q^2 - - monitoring data noise or variance;
λ_* - - test channel (unestablished connection) wavelength;
Target:
Q_* - - unestablished connection OSNR prediction;
Algorithm:
$\mathbf{L} := Cholesky(\mathbf{K})$; [40]
$\mathbf{A} := \mathbf{L}^T\backslash(\mathbf{L}\backslash\mathbf{Q})$ - - intermediate computation;
$\overline{Q_*} := \mathbf{K}_*^{\mathbf{T}}\mathbf{A}$ - - posterior OSNR mean;
$\mathbf{B} := \mathbf{L}\backslash\mathbf{K}_*^{\mathbf{T}}$ - - intermediate computation;
$Cov[Q_*] := \mathbf{K}_{**} - \mathbf{B}^T\mathbf{B}$ - - posterior OSNR variance;
$\log[p(\mathbf{Q}|\lambda)] := -\frac{1}{2}\mathbf{Q}^T\mathbf{A} - \sum_i^n \log \mathbf{L}_{\mathbf{i}} - \frac{n}{2}\log 2\pi$ - - log marginal likelihood to be maximized during hyperparameter tuning;
Return:
$\overline{Q_*}$, $Cov[Q_*]$, $\log[p(\mathbf{Q}|\lambda)]$

Algorithm 1: GP learning of noise spectrum

$$ECI = \overline{Q_*} \pm 1.96\sqrt{Cov[Q_*]} \tag{15}$$

B. Bayesian optimization

Each time a single channel is monitored, the control strategy of the monitoring device based on the MoD architecture follows a "self-taught" monitoring process. Bayesian optimization (BO) determines the next channel to be monitored (λ_{next}) based on learning from the OSNR performance that has been monitored so far. Fig. 5 shows the flow chart of the overall learning model [20].

BO is intrinsically a decision trade-off algorithm on top of GP ECI. A large ECI area is an indicator for a high variance. The bounded region becomes more explorable because of the high estimation uncertainty. In the meantime, since we are only interested in the worst case OSNR performance, i.e., the global maximum point of OSNR degradation per link, the region around the monitored high OSNR degradation values (high mean) is likely to contain a worse value. Therefore we should also exploit this high mean region. Here we define that for link i connecting node j and $j+1$, the OSNR degradation in dB is

$$OSNR^i_{deg} = OSNR^j - OSNR^{j+1} \tag{16}$$

To fit BO to GP, a utility (or acquisition) function "probability of improvement" (PI) [41] is used to deal with this fundamental exploration and exploitation trade-off. PI computes the probability of establishing the next probe channel to be monitored as

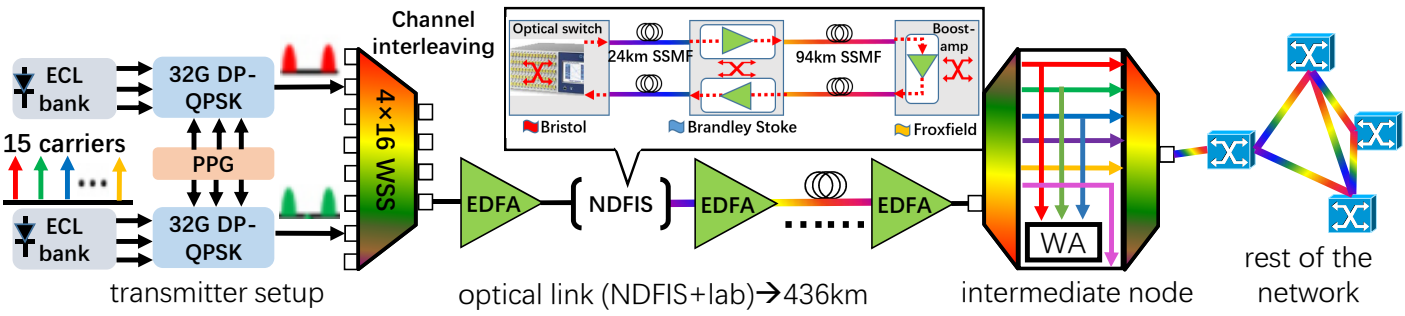

Figure 4: Field trial testbed using NDFIS, signals are transmitted from Bristol to Froxfield and looped back to Bristol, the detailed intermediate node architecture is shown in Fig. 2, ECL (external cavity laser), PPG (pulse pattern generator), DP-QPSK (dual polarization quadrature phase shift keying), SSMF (standard single mode fiber)

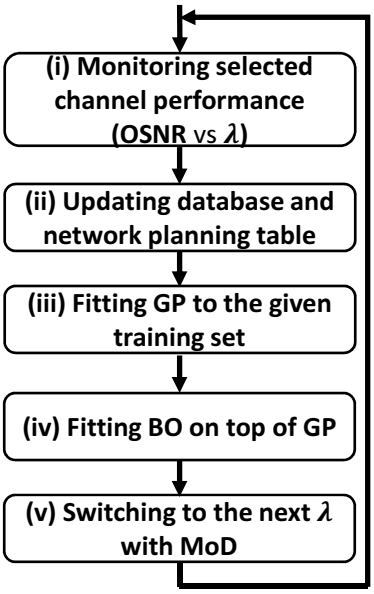

Figure 5: Monitoring on-demand strategy driven by Bayesian optimization.

Input:
$t = 1 : n$ - - total number of channels;
$\mathbf{D}[\lambda(wavelength), OSNR]$ - - GP regression of channel OSNR;
$\sigma_Q^2, \mathbf{K}$ - - GP kernel function and monitoring variance;
Target: λ_t - - next probing channel;
Algorithm:
for t = 1,2,...,n **do** {
find λ_t by combining attributes of the posterior distribution in the PI function U_{PI} and maximizing
$\lambda_t = \text{argmax}_\lambda[U_{PI}(\lambda|\mathbf{D}_{1:t-1})]$
monitor the objective value OSNR(λ_t)
augment the data set
$\mathbf{D}_{1:t} = \{\mathbf{D}_{1:t-1}, [\lambda_t, OSNR(\lambda_t)]\}$
update GP
} **end for**
Return: λ_t, $\mathbf{D}_{1:t}$

Algorithm 2: BO-driven MoD function for channel selection

$$U_{PI}(\lambda_{next}; D_n) := Pr[OSNR(\lambda_{next}) > \mu^+_{OSNR}] = \Phi[(\mu_n(\lambda_{next}) - \mu^+_{OSNR})/\sigma_n(\lambda_{next})] \quad (17)$$

where μ^+_{OSNR} is the worst $OSNR_{deg}$ that has been monitored so far, $\mu_n(\lambda_{next})$ and $\sigma_n(\lambda_{next})$ represent the posterior GP returned $OSNR_{deg}$ mean (quantified degree of exploitation) and variance (quantified degree of exploration), Φ is the standard cumulative distribution function. PI returns the area under the posterior Gaussian distribution above μ^+_{OSNR}, the larger the area, the higher probability of improvement. The point with the highest probability of improvement (the maximal expected utility) is selected [42]. BO returns the next optimized monitoring or probing choice λ_{next} by maximizing the utility function U_{PI}. The pseudocode of BO-driven MoD function is summarized in Algorithm 2.

IV. Field Trial Testbed and Result

A. Field trial experiment

Fig. 4 depicts the field trial network using part of the UK National Dark Fiber Infrastructure Service (NDFIS). NDFIS allows experiments to be carried out in a real-world operating network, hence introducing sufficient operational uncertainties. 16 equalized 50GHz/0.4nm-spaced 32Gbaud DP-QPSK signals are available at the transmitter side and ready to be launched into the network. Channel power is set to 0 dBm/channel/span by each EDFA to avoid unwanted nonlinear distortion. Signals first enter the NDFIS link running from Bristol to Brandley Stoke and further to Froxfield which gives 236km effective loop-back transmission distance. Another 200km fiber link (lab-based) is connected after the loop-back (giving 436km in total) where signals are amplified every 50km. Launch OSNR is kept identical (30dB) to simplify

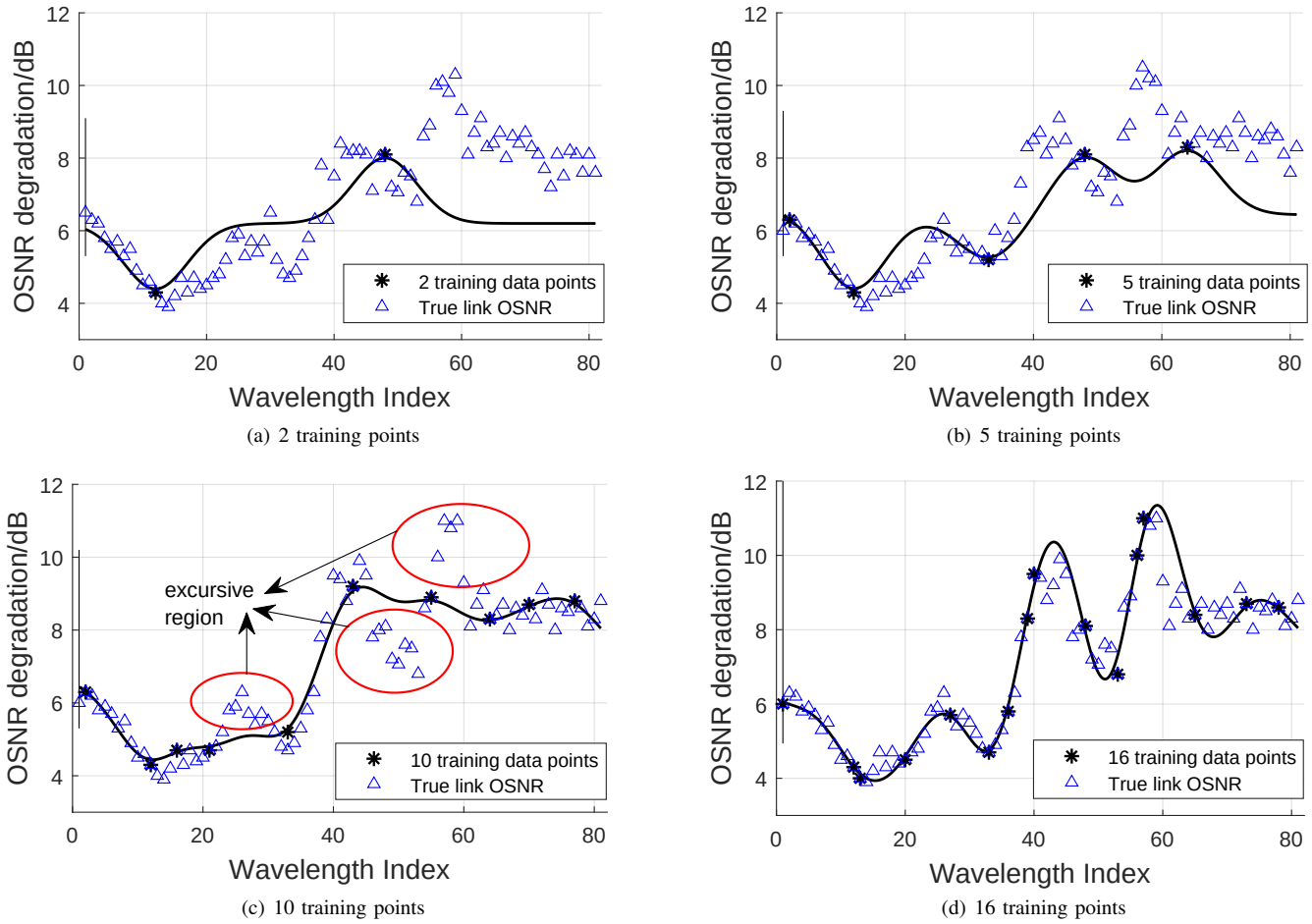

(a) 2 training points (b) 5 training points

(c) 10 training points (d) 16 training points

Figure 6: GP prediction of unestablished channel OSNR performance with (a) 2 training points, (b) 5 training points, (c) 10 training points, (d) 16 training points.

the computation of our scenario. Channels with different wavelengths undergo different OSNR degradations after the link. This can be visualized by the non-uniformity of the OSNR curve as shown in Fig. 6. We treat the transmitter as the first node, MoD is performed in the intermediate node where signals pass WSS (add-drop), coupler (tapping power), filter (selecting the channel of interest), and enter WA for in-band OSNR monitoring.

The WA monitoring device can be either shared among different fiber links by switching the optical switch ports, or among different channels in the same link by controlling the filter. In this work we are focused on the latter case. The exploration and exploitation trade-off is made to find the worst OSNR performance of a specific link with as few monitoring trials as possible. Our target is to find $max[OSNR^i_{deg}]$, in this experimental setup this is equal to finding $max[30dB - OSNR^{j+1}]$ according to equation 16 where $OSNR^{j+1}$ is the $(j+1)$th intermediate node to be monitored.

It is worth noting that our proposed method is also applicable to mesh networks, i.e., with different signal launch OSNR at the beginning of each link. As section II describes, we are able to monitor any intermediate node $OSNR^j$, this makes the calculation of OSNR degradation possible for each

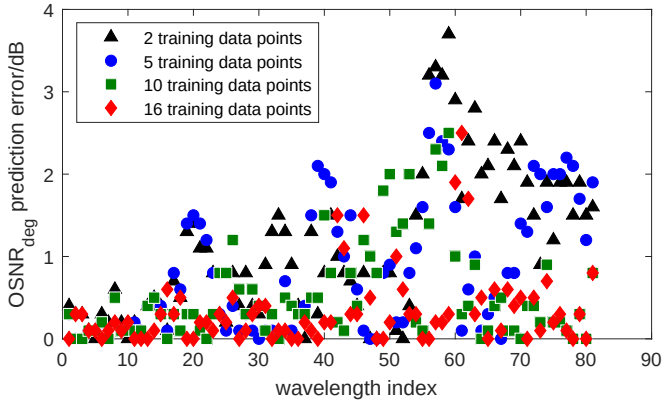

Figure 7: OSNR degradation prediction error with different GP training data sets.

individual link using equation 16. If we are interested in the lightpath metric, we can simply sum up the degradations of the traversed links. Or we can use the following equation [19]

$$\frac{1}{OSNR_{path}} = \sum_{i=1}^{n} \frac{1}{OSNR_{link-i}} \tag{18}$$

where $OSNR_{link-i}$ is the end-to-end OSNR for link i. This assumes that ASE noise is linearly accumulated throughout the lightpath. The linear operation regime is assumed. If an unestablished signal OSNR is unknown for a specific link, we can use the proposed GP regression method to infer the OSNR for the wavelength in that link.

B. GP performance evaluation

BO computes PI according to GP ECI (selection of the next channel to be monitored). The global OSNR degradation maximum point is estimated by further GP regression with the newly monitored data. It is necessary to evaluate the performance of GP prediction for unestablished channel OSNR with limited online monitoring data.

Fig. 6(a) - 6(d) show the GP predictions of un-established channel OSNR under different link loading and monitoring conditions. Wavelength is indexed into 1 to 81 representing 1562.6nm to 1530.7nm at 0.4nm grid (ITU 50GHz). Hyper-parameters are optimized to be $\sigma_f^2 = 2.07$ and $l = 1.53$. All the OSNR reference values are used as test data to evaluate the corresponding GP prediction accuracy. We define the link true OSNR as the OSNR values that are monitored by our proposed in-band method rather than predicted by any models. The OSNR test data is measured by setting up a single test channel at each of the empty wavelength slot. It is torn down each time the reference value is recorded. Due to cascaded EDFA power amplification characteristics, the link OSNR performance varies with the loading status. By setting up only a single test channel, the impact of channel loading to EDFA is kept to minimum. Fig. 6(a) has only two monitoring/training channels, it can be seen that the fitted GP curve can hardly capture the link OSNR performance due to too few training data points available. Fig. 6(b) and Fig. 6(c) increase the data point size to 5 and 10 respectively, each shows relative improvement in capturing the true link OSNR behavior. However, the performance is still poor in some excursive regions including the global maximum point. Finally GP is able to predict the whole link OSNR with reasonable accuracy when the number of training channels reaches 16, as shown in Fig. 6(d). The prediction error for each training case is shown in Fig. 7, training cases with 2 training points, 5 training points, 10 training points and 16 training points have root mean squared error (RMSE) of 1.5dB, 1.2dB, 0.8dB and 0.5dB respectively. This means that adequate online monitoring data is essential to capture accurate link OSNR performance.

It is worth noting that, without involving the self-taught MoD function, GP prediction with randomly generated training set does not guarantee that the current estimated global maximum point is the true target value, i.e., the worst OSNR degradation of the link. The only way to gain confidence about this estimation is to use as many monitoring data points as possible for training. Such amount of online monitoring data is hard to obtain without sending monitoring probes. In the case of active monitoring, the number of monitoring probes should be optimized to avoid interruption to existing services.

C. Self-taught MoD

By applying BO on top of GP, the next monitoring channel of interest depends on the ECI computed by GP posterior mean and variance as well as the current global maxima monitoring points. Fig. 8(a) and Fig. 8(b) show the details of BO process. Different monitoring decisions are made depending on the normalized acquisition function (AF) u_{PI} computed by PI. The cyan region represents the estimation uncertainty (95% confidence integral) which goes high where there is no monitoring data, and goes low where there is monitoring data. The next channel of interest (next best guess) is marked by a star on the AF curve. In Fig. 8(a) which contains 4 monitoring points, the algorithm tends to prioritize exploration given the 4 points spread in large ranges across the wavelength band. So the indicated next best guess locates in high ECI region. After 5 steps, in Fig. 8(b), the algorithm starts to exploit the region with high posterior mean according to GP. The indicated next best guess no longer locates in high ECI region but in high mean region. As more channels are monitored and utilized to be the next step GP training data, the BO decision will be made around the global maxima. It is worth mentioning that due to the stochastic function sampling process of GP, each time BO re-runs, the posterior mean and variance may differ from the previous value. So the choice for the next channel of interest may vary.

Fig. 8(c) evaluates the number of filter switching times required to find $OSNR_{deg}$ global maximum point. As mentioned in section II, the in-band OSNR monitoring device can only compute a single channel OSNR. So selection of the next channel of interest is done by configuring the filter (or WSS profile for our experiment) in the MoD architecture. Two other switching strategies are used to assess the performance of MoD: 1. Sequential monitoring (SM): sequentially switching to each channel in the link from left to right; 2. Random monitoring (RM): the switching or monitoring order is stochastic. Note that by using SM and RM strategies, active probing method becomes clumsy since the required monitoring probe has to loop across the whole C band without optimization. In the case of 16 channels monitoring (Fig. 6(d)), with a total number of 40 switching times, BO first finds the highest OSNR degradation located at $\lambda = 1540.2$nm (wavelength index #59) with 8 switching times. It is 62.5% quicker than SM (13 times) and 400% quicker than RM (40 times). 75% of the BO data (after 8 switching times) is constant when searching for the worst OSNR degradation (11dB). This means the rest of the constant data can be omitted after the first detection, resulting in 50% data saving (8 channels out of 16). This demonstrates that BO can take the monitoring process out of the loop by intelligently selecting the channels that provide the largest information gain.

Fig. 8(d) demonstrates the capability of BO in locating the target OSNR with "just enough" monitoring data. The complete link OSNR performance for each wavelength slot is tested and recorded as benchmark data. The fitted GP curve using BO has the posterior global maximum at exactly the same point as using all the 16 training channels. BO achieves only 0.5dB prediction error (relative to the reference value)

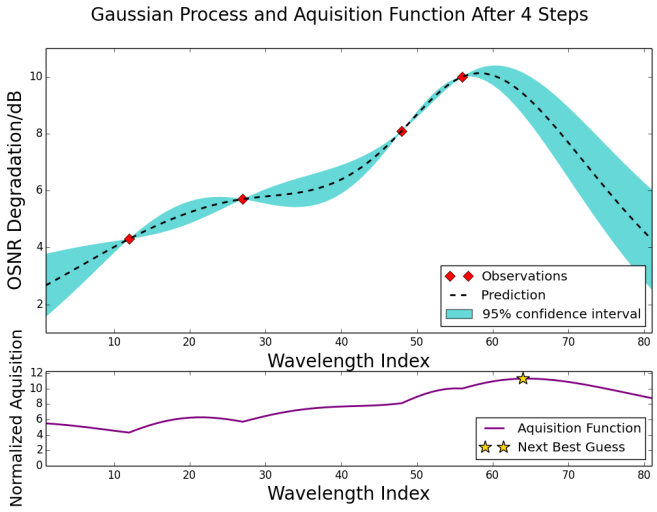

(a) GP and AF after 4 monitoring trials

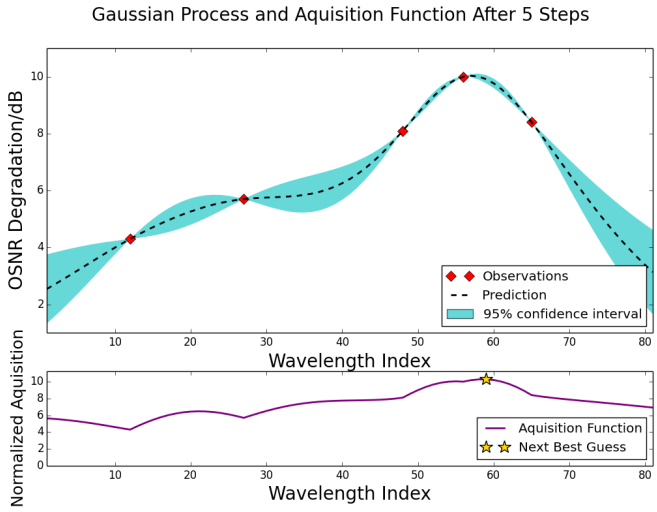

(b) GP and AF after 5 monitoring trials

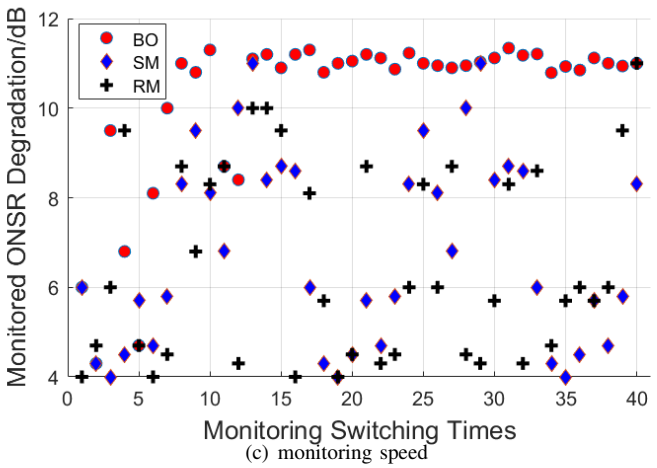

(c) monitoring speed

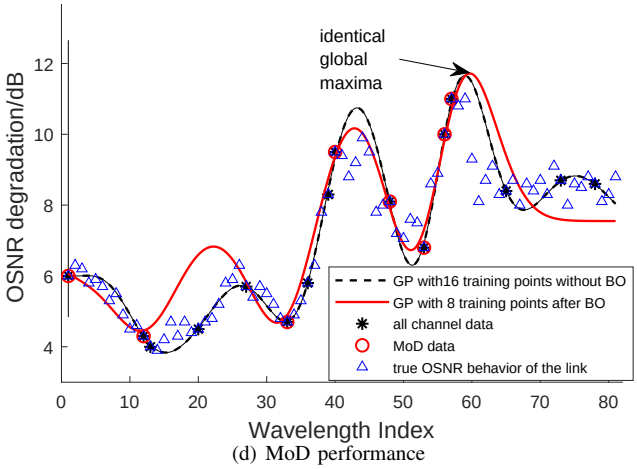

(d) MoD performance

Figure 8: (a) BO-driven MoD after GP fitting with 4 training points, the algorithm tends to explore high ECI region. (b) BO-driven MoD after GP fitting with 5 training points, the algorithm starts to exploit high posterior mean region as indicated by the normalized acquisition function. (c) Monitoring performance in terms of switching times taken to find the global maximum, (d) prediction of $OSNR_{deg}$ global maximum with MoD (8 monitoring trials) and complete GP fitting (16 monitoring trials)

for the target OSNR while the data needed is halved. This proves the capability of MoD in retrieving the most critical OSNR information with up to 91% data saving (8 out of 88 if C band is fully loaded), and in the mean time, retaining identical prediction accuracy compared to full exploration with 16 channels.

V. Summary

In this field trial we have demonstrated a self-taught monitoring-on-demand function driven by Bayesian optimization at network intermediate nodes. A single in-band OSNR monitoring device is shared among different channels. We first present an in-band OSNR monitoring algorithm implemented in a high-resolution OSA which can be dynamically switched to monitor any channel on-demand. The algorithm takes back-to-back signal spectrum as reference spectrum together with real-time offset monitoring power to compute target in-band OSNR value. The algorithm achieves OSNR monitoring accuracy of 0.6dB with 1GHz device frequency resolution. With such monitoring capability, Bayesian optimization is then applied to learn from already established connections. It aims to minimize the number of monitoring trials needed for locating the worst OSNR degradation of the link. It has been shown that by using pure GP regression, at least 16 sparsely distributed monitoring channels are required to completely capture the whole link OSNR performance (including the global maximum). BO significantly accelerates the process with only 8 monitoring trials to efficiently search for the target OSNR value. In situations where active monitoring probe has to be used, BO is expected to save up to 91% of the monitoring trials (whole C band channels) while accurately predicting the global maximum with 0.5dB error. Such intelligent self-taught learning strategy enables a data-efficient, out-of-the-loop monitoring process. It can be critical in accelerating the monitoring process and saving the number of probe signals for active monitoring purposes.

ACKNOWLEDGMENT

This work is supported by EPSRC grant EP/L020009/1: TOUCAN and EP/L026155/2: INSIGHT project.

REFERENCES

[1] M. Cantono, R. Gaudino, and V. Curri, "Potentialities and criticalities of flexible-rate transponders in DWDM networks: A statistical approach," *IEEE/OSA Journal of Optical Communications and Networking*, vol. 8, pp. A76–A85, July 2016.

[2] D. A. Morero, M. A. Castrillón, A. Aguirre, M. R. Hueda, and O. E. Agazzi, "Design tradeoffs and challenges in practical coherent optical transceiver implementations," *Journal of Lightwave Technology*, vol. 34, no. 1, pp. 121–136, 2016.

[3] Y. Li, L. Gao, G. Shen, and L. Peng, "Impact of ROADM colorless, directionless, and contentionless (CDC) features on optical network performance [invited]," *IEEE/OSA Journal of Optical Communications and Networking*, vol. 4, pp. B58–B67, Nov 2012.

[4] T. Panayiotou, S. P. Chatzis, and G. Ellinas, "Performance analysis of a data-driven quality-of-transmission decision approach on a dynamic multicast-capable metro optical network," *Journal of Optical Communications and Networking*, vol. 9, no. 1, pp. 98–108, 2017.

[5] Z. Dong, F. N. Khan, Q. Sui, K. Zhong, C. Lu, and A. P. T. Lau, "Optical performance monitoring: A review of current and future technologies," *Journal of Lightwave Technology*, vol. 34, pp. 525–543, Jan 2016.

[6] Y. Pointurier, M. Coates, and M. Rabbat, "Cross-layer monitoring in transparent optical networks," *Journal of Optical Communications and Networking*, vol. 3, no. 3, pp. 189–198, 2011.

[7] C. V. Saradhi and S. Subramaniam, "Physical layer impairment aware routing (PLIAR) in WDM optical networks: issues and challenges," *IEEE Communications Surveys & Tutorials*, vol. 11, no. 4, 2009.

[8] H. Braham, S. B. Jemaa, B. Sayrac, G. Fort, and E. Moulines, "Low complexity spatial interpolation for cellular coverage analysis," in *Modeling and Optimization in Mobile, Ad Hoc, and Wireless Networks (Wiopt), 2014 12Th International Symposium On*, pp. 188–195, IEEE, 2014.

[9] F. Meng, Y. Ou, S. Yan, K. Sideris, M. D. G. Pascual, R. Nejabati, and D. Simeonidou, "Field trial of a novel SDN enabled network restoration utilizing in-depth optical performance monitoring assisted network re-planning," in *2017 Optical Fiber Communications Conference and Exhibition (OFC)*, pp. 1–3, March 2017.

[10] L. Cui, F. R. Yu, and Q. Yan, "When big data meets software-defined networking: SDN for big data and big data for SDN," *IEEE Network*, vol. 30, pp. 58–65, January 2016.

[11] O. Grytsenko and V. Sayenko, "A method of network monitoring with reduced measured data," in *Scientific-Practical Conference Problems of Infocommunications. Science and Technology (PIC S&T), 2017 4th International*, pp. 477–482, IEEE, 2017.

[12] R. Borkowski, R. J. Durán, C. Kachris, D. Siracusa, A. Caballero, N. Fernández, D. Klonidis, A. Francescon, T. Jiménez, J. C. Aguado, I. d. Miguel, E. Salvadori, I. Tomkos, R. M. Lorenzo, and I. T. Monroy, "Cognitive optical network testbed: EU project CHRON," *Journal of Optical Communications and Networking*, vol. 7, no. 2, pp. A344–A355, 2015.

[13] W. Xiaolin, Q. Xiaogang, and L. Lifang, "Probe selection algorithm for faulty links localization in all-optical networks," in *Smart Grid and Electrical Automation (ICSGEA), 2017 International Conference on*, pp. 269–272, IEEE, 2017.

[14] H.-T. Luk and L.-K. Chen, "Active probing assisted monitoring for software defined networks," in *Optical Fiber Communications Conference and Exhibition (OFC), 2015*, pp. 1–3, IEEE, 2015.

[15] A. E. Willner and S.-M. Hwan, "Transmission of many WDM channels through a cascade of EDFA's in long-distance links and ring networks," *Journal of Lightwave Technology*, vol. 13, pp. 802–816, May 1995.

[16] R. Giridhar Kumar, I. Sadhu, and N. Sangeetha, "Gain and noise figure analysis of erbium doped fiber amplifier by four stage enhancement and analysis," *International Journal of Scientific and Research Publications*, vol. 4, no. 4, 2014.

[17] Y. Huang, C. L. Gutterman, P. Samadi, P. B. Cho, W. Samoud, C. Ware, M. Lourdiane, G. Zussman, and K. Bergman, "Dynamic mitigation of EDFA power excursions with machine learning," *Optics Express*, vol. 25, no. 3, pp. 2245–2258, 2017.

[18] L. Barletta, A. Giusti, C. Rottondi, and M. Tornatore, "QoT estimation for unestablished lighpaths using machine learning," in *Optical Fiber Communication Conference*, pp. Th1J–1, Optical Society of America, 2017.

[19] S. Oda, M. Miyabe, S. Yoshida, T. Katagiri, Y. Aoki, T. Hoshida, J. C. Rasmussen, M. Birk, and K. Tse, "A learning living network with open ROADMs," *Journal of Lightwave Technology*, vol. 35, no. 8, pp. 1350–1356, 2017.

[20] F. Meng, A. Mavromatis, Y. Bi, Y. Ou, K. Nikolovgenis, R. Nejabati, and D. E. Simeonidou, "Field trial of monitoring on-demand at intermediate-nodes through bayesian optimization," in *Optical Fiber Communication Conference*, pp. M3A–2, Optical Society of America, 2018.

[21] S. Oda, J. Y. Yang, Y. Akasaka, K. Sone, Y. Aoki, M. Sekiya, and J. C. Rasmussen, "In-band OSNR monitor using an optical bandpass filter and optical power measurements for superchannel signals," in *39th European Conference and Exhibition on Optical Communication (ECOC 2013)*, pp. 1–3, Sept 2013.

[22] Z. Dong, K. Zhong, X. Zhou, C. Lu, A. P. T. Lau, Y. Lu, and L. Li, "Modulation-format-independent OSNR monitoring insensitive to cascaded filtering effects by low-cost coherent receptions and RF power measurements," *Optics express*, vol. 23, no. 12, pp. 15971–15982, 2015.

[23] G. Yin, S. Cui, C. Ke, and D. Liu, "Reference optical spectrum based in-band OSNR monitoring method for EDFA amplified multispan optical fiber transmission system with cascaded filtering effect," *IEEE Photonics Journal*, vol. 10, pp. 1–10, June 2018.

[24] M. R. Chitgarha, S. Khaleghi, W. Daab, M. Ziyadi, A. Mohajerin-Ariaei, D. Rogawski, M. Tur, J. Touch, V. Vusirikala, W. Zhao, and A. Willner, "Demonstration of wdm OSNR performance monitoring and operating guidelines for pol-muxed 200-Gbit/s 16-QAM and 100-Gbit/s QPSK data channels," in *Optical Fiber Communication Conference and Exposition and the National Fiber Optic Engineers Conference (OFC/NFOEC), 2013*, pp. 1–3, IEEE, 2013.

[25] A. Almaiman, M. R. Chitgarha, W. Daab, M. Ziyadi, A. Mohajerin-Ariaei, S. Khaleghi, M. Willner, V. Vusirikala, X. Zhao, D. Kilper, L. Paraschis, A. Ahsan, M. Wang, K. Bergman, M. Tur, J. D. Touch, and A. E. Willner, "Experimental demonstration of robustness and accuracy of a DLI-based OSNR monitor under changes in the transmitter and link for different modulation formats and baud rates," *Optics letters*, vol. 40, no. 9, pp. 2012–2015, 2015.

[26] N. Amaya, G. S. Zervas, and D. Simeonidou, "Architecture on demand for transparent optical networks," in *Transparent Optical Networks (ICTON), 2011 13th International Conference on*, pp. 1–4, IEEE, 2011.

[27] Finisar, *WaveAnalyzer 1500S*. https://www.finisar.com/optical-instrumentation/waveanalyzer-1500s-high-resolution-optical-spectrum-analyzer.

[28] W. Moench, J. Larikova, and P. Winterling, "In-service measurement of the OSNR in ROADM-based networks," in *Photonic Networks, 2008 ITG Symposium on*, pp. 1–3, VDE, 2008.

[29] N. Amaya, G. S. Zervas, and D. Simeonidou, "Architecture on demand for transparent optical networks," in *2011 13th International Conference on Transparent Optical Networks*, pp. 1–4, June 2011.

[30] A. E. Willner and S.-M. Hwan, "Transmission of many WDM channels through a cascade of EDFA's in long-distance links and ring networks," *Journal of lightwave technology*, vol. 13, no. 5, pp. 802–816, 1995.

[31] J.-X. Cai, K.-M. Feng, X. Chen, and A. Willner, "Equalization of nonuniform EDFA gain using a fiber-loop mirror," *IEEE Photonics Technology Letters*, vol. 9, no. 7, pp. 916–918, 1997.

[32] C. A. Marques, R. A. Oliveira, A. A. Pohl, and R. N. Nogueira, "Adjustable EDFA gain equalization filter based on a single lpg excited by flexural acoustic waves for future DWDM networks," in *International Conference on Fibre Optics and Photonics*, pp. W2A–3, Optical Society of America, 2012.

[33] P. Schiopu and F. Vasile, "The EDFA performance with gain versus pump power," in *Semiconductor Conference, 2004. CAS 2004 Proceedings. 2004 International*, vol. 1, IEEE, 2004.

[34] M. Li, W. Jiao, Y. Song, X. Zhang, S. Dong, and Y. Poo, "Investigation of the EDFA effect on the BER performance in space uplink optical communication under the atmospheric turbulence," *Optics Express*, vol. 22, no. 21, pp. 25354–25361, 2014.

[35] W. Mo, C. L. Gutterman, Y. Li, S. Zhu, G. Zussman, and D. C. Kilper, "Deep-neural-network-based wavelength selection and switching in ROADM systems," *Journal of Optical Communications and Networking*, vol. 10, no. 10, pp. D1–D11, 2018.

[36] S. Yan, F. N. Khan, A. Mavromatis, D. Gkounis, Q. Fan, F. Ntavou, K. Nikolovgenis, F. Meng, E. H. Salas, C. Guo, C. Lu, A. P. T. Lau, R. Nejabati, and D. Simeonidou, "Field trial of machine-learning-assisted and SDN-based optical network planning with network-scale monitoring database," in *43rd European Conference on Optical Communication (ECOC 2017)*, 2017.

[37] F. Meng, K. Nikolovgenis, Y. Ou, Y. Bi, E. H. Salas, R. Nejabati, and D. E. Simeonidou, "Field trial of gaussian process learning of function-

agnostic channel performance under uncertainty," in *Optical Fiber Communication Conference*, pp. W4F–5, Optical Society of America, 2018.
[38] Ebden, "Gaussian processes for regression: A quick introduction," *The Website of Robotics Research Group in Department on Engineering Science, University of Oxford*, vol. 91, pp. 424–436, 2008.
[39] C. E. Rasmussen and H. Nickisch, "Gaussian processes for machine learning (GPML) toolbox," *Journal of Machine Learning Research*, vol. 11, no. Nov, pp. 3011–3015, 2010.
[40] A. Krishnamoorthy and D. Menon, "Matrix inversion using cholesky decomposition," in *Signal Processing: Algorithms, Architectures, Arrangements, and Applications (SPA), 2013*, pp. 70–72, IEEE, 2013.
[41] B. Shahriari, K. Swersky, Z. Wang, R. P. Adams, and N. De Freitas, "Taking the human out of the loop: A review of bayesian optimization," *Proceedings of the IEEE*, vol. 104, no. 1, pp. 148–175, 2016.
[42] J. Snoek, H. Larochelle, and R. P. Adams, "Practical bayesian optimization of machine learning algorithms," in *Advances in neural information processing systems*, pp. 2951–2959, 2012.

PLACE PHOTO HERE

Michael Shell Biography text here.

John Doe Biography text here.

Jane Doe Biography text here.